Perinatal deiodinase 2 expression in hepatocytes defines epigenetic susceptibility to liver steatosis and obesity

Tatiana L. Fonseca[a], Gustavo W. Fernandes[a,b], Elizabeth A. McAninch[a], Barbara M. L. C. Bocco[a,b], Sherine M. Abdalla[c], Miriam O. Ribeiro[d], Petra Mohácsik[e,f], Csaba Fekete[e,g], Daofeng Li[h], Xiaoyun Xing[h], Ting Wang[h], Balázs Gereben[e], and Antonio C. Bianco[a,1]

[a]Division of Endocrinology and Metabolism, Rush University Medical Center, Chicago, IL 60612; [b]Translational Medicine, Federal University of São Paulo, São Paulo 04023-900, SP, Brazil; [c]Department of Medicine, University of Miami Miller School of Medicine, Miami, FL; 33136; [d]Developmental Disorders Program, Center of Biological Science and Health, Mackenzie Presbyterian University, São Paulo 01302-907, SP, Brazil; [e]Department of Endocrine Neurobiology, Institute of Experimental Medicine, Hungarian Academy of Sciences, 1083 Budapest, Hungary; [f]János Szentágothai School of Neurosciences, Semmelweis University, 1085 Budapest, Hungary; [g]Division of Endocrinology, Diabetes and Metabolism, Tufts Medical Center, Boston, MA 02116; and [h]Department of Genetics, Center for Genome Sciences and Systems Biology, Washington University School of Medicine, St. Louis, MO 63108

Edited by Steven A. Kliewer, The University of Texas Southwestern Medical Center at Dallas, Dallas, TX, and approved September 21, 2015 (received for review May 11, 2015)

Thyroid hormone binds to nuclear receptors and regulates gene transcription. Here we report that in mice, at around the first day of life, there is a transient surge in hepatocyte type 2 deiodinase (D2) that activates the prohormone thyroxine to the active hormone triiodothyronine, modifying the expression of ∼165 genes involved in broad aspects of hepatocyte function, including lipid metabolism. Hepatocyte-specific D2 inactivation (ALB-D2KO) is followed by a delay in neonatal expression of key lipid-related genes and a persistent reduction in peroxisome proliferator-activated receptor-γ expression. Notably, the absence of a neonatal D2 peak significantly modifies the baseline and long-term hepatic transcriptional response to a high-fat diet (HFD). Overall, changes in the expression of approximately 400 genes represent the HFD response in control animals toward the synthesis of fatty acids and triglycerides, whereas in ALB-D2KO animals, the response is limited to a very different set of only approximately 200 genes associated with reverse cholesterol transport and lipase activity. A whole genome methylation profile coupled to multiple analytical platforms indicate that 10–20% of these differences can be related to the presence of differentially methylated local regions mapped to sites of active/suppressed chromatin, thus qualifying as epigenetic modifications occurring as a result of neonatal D2 inactivation. The resulting phenotype of the adult ALB-D2KO mouse is dramatic, with greatly reduced susceptibility to diet-induced steatosis, hypertriglyceridemia, and obesity.

deiodinase | thyroid hormone | lipids | steatosis | obesity

The active thyroid hormone triiodothyronine (T3) plays multiple metabolic roles, affecting gene expression in vertebrates (1). In contrast to other metabolically relevant hormones, serum T3 levels are relatively stable throughout life (2), except during caloric restriction or life-threating illness (3). This suggests that important T3-dependent metabolic pathways are not controlled through changes in circulating levels of the hormone.

The key to metabolic control by thyroid hormone lies in the deiodinases (4). These are enzymes that can either activate or inactivate thyroid hormone at the target cell level, changing intracellular T3 levels without necessarily affecting circulating T3 levels. For example, local T3 production via type 2 deiodinase (D2) is greatly accelerated in brown adipose tissue (BAT) during cold exposure, activating T3-dependent gene transcription (5). In contrast, in the ischemic/hypoxic myocardium and cerebrum, both T3 and thyroxine (T4) are inactivated by type 3 deiodinase (D3) (6, 7), locally reducing thyroid hormone signaling and T3-mediated metabolic pathways (8).

The liver is a canonical target of thyroid hormone, with T3 stimulating lipogenesis, fatty acid oxidation, bile acid, and cholesterol metabolism (9). In addition, clinical studies have shown that thyrotoxicosis increases hepatic glucose production and reduces hepatic insulin sensitivity (10, 11). Thyroid hormone receptor β is the most abundant isoform present in the liver (12), and various T3-responsive genes have been identified in this organ (13). In turn, the liver is also a site for thyroid hormone inactivation through conjugation and deiodination via the D1 pathway (14, 15).

D2 expression is found in the chicken liver (16) and during the early stages of metamorphosis of the amphibian (17). D2 is not expressed in the mammalian liver, except for the D2 found in mouse liver macrophages (18). Nevertheless, a mouse with target disruption of liver X receptor (LXR) α and LXRβ exhibits ectopic liver D2 expression in response to feeding with western diet-induced (19). Consistent with a role for LXR/retinoid X receptor, subsequent studies revealed that the human DIO2 promoter is negatively regulated by both 22(R)-OH-cholesterol and 9-cis RA, which is not observed in the chicken liver (20).

Global inactivation of D2 (global-D2KO) causes liver steatosis, which is most severe during high-fat feeding and acclimatization to thermoneutrality (21); however, given that D2 is not normally found in adult mouse liver, such a phenotype has been attributed to an indirect metabolic role played by D2 in other tissues, such as brain, BAT, and/or skeletal muscle (22). Here we report the phenotypic characterization, as well as the liver transcriptome and methylome, of a mouse with hepatocyte-specific D2KO (ALB-D2KO).

Significance

Thyroid hormone is secreted mostly as a prohormone that must be activated to gain biological activity. The activation reaction is the removal of one iodine atom, i.e., deiodination of thyroxine to active thyroid hormone triiodothyronine (T3), which is catalyzed by a group of enzymes known as deiodinases. These enzymes control the amounts of intracellular and circulating T3. Here we report that in mice, there is a brief neonatal surge in hepatocyte type 2 deiodinase (D2) that transiently stimulates liver expression of lipid-related genes. The surge in D2 also affects the pattern of DNA methylation and responsiveness of lipid-related genes, modifying metabolic susceptibility to liver steatosis, hypertriglyceridemia, and obesity.

Author contributions: T.L.F. and A.C.B. designed research; T.L.F., G.W.F., B.M.L.C.B., S.M.A., P.M., D.L., and X.X. performed research; C.F. and B.G. contributed new reagents/analytic tools; T.L.F., G.W.F., E.A.M., B.M.L.C.B., S.M.A., M.O.R., T.W., and A.C.B. analyzed data; and T.L.F. and A.C.B. wrote the paper.

The authors declare no conflict of interest.

This article is a PNAS Direct Submission.

[1]To whom correspondence should be addressed. Email: abianco@deiodinase.org.

This article contains supporting information online at www.pnas.org/lookup/suppl/doi:10.1073/pnas.1508943112/-/DCSupplemental.

Results

D2 Is Expressed in Fetal and Neonatal Mouse Liver. D2 mRNA was detected by quantitative RT-PCR (qRT-PCR) as early as embryonic day (E) 12 and increased progressively by approximately threefold on postnatal day (P) 1, a time at which there is marked expansion of hepatocytes in the embryonic liver. Subsequently, D2 mRNA decreased and became undetectable during adulthood (Fig. 1*A*). In situ hybridization studies detected the presence of D2 mRNA in the liver of P1 mice (Fig. 1 *B–D*), but only background levels in the adult liver (Fig. 1 *G* and *H*). D2 activity was readily detectable in neonatal liver, but was absent in the adult liver (Fig. 1*I*). In contrast, the hepatic expression of the inactivating deiodinase D3 fluctuated in the embryonic and perinatal periods and dropped to undetectable levels during adulthood (*SI Appendix*, Fig. S1*A*). In contrast, D1 expression increased progressively from E12 to a ∼2,000-fold peak level during adulthood (*SI Appendix*, Fig. S1*B*).

We next crossed the flox-D2 mouse with the Cre-Albumin mouse, a promoter expressed exclusively in hepatocytes (23). There is minimal albumin expression at E15.5 in liver, with much stronger expression seen at around P3, when the majority of the differentiated liver cells are hepatocytes (23). Whereas ALB-D2KO animals exhibited normal hepatic D2 expression during embryonic life (Fig. 1*A*), hepatic D2 mRNA levels in P1 animals were one-half (Fig. 1*A*) and D2 activity was less than one-half (Fig. 1*I*), decreasing T3 production by approximately 25% (Fig. 1*J*) and T3 content by approximately one-half (Fig. 1*K*). The fact that not all D2 expression was eliminated in the ALB-D2KO animals compared with global-D2KO livers (Fig. 1*I*) indicates that D2 is also expressed in albumin-negative liver cells, which also subsides after birth. Note that the normal loss of D2 activity observed in control animals at P5 resulted in an approximate 65% decrease in liver T3 content (Fig. 1*J*).

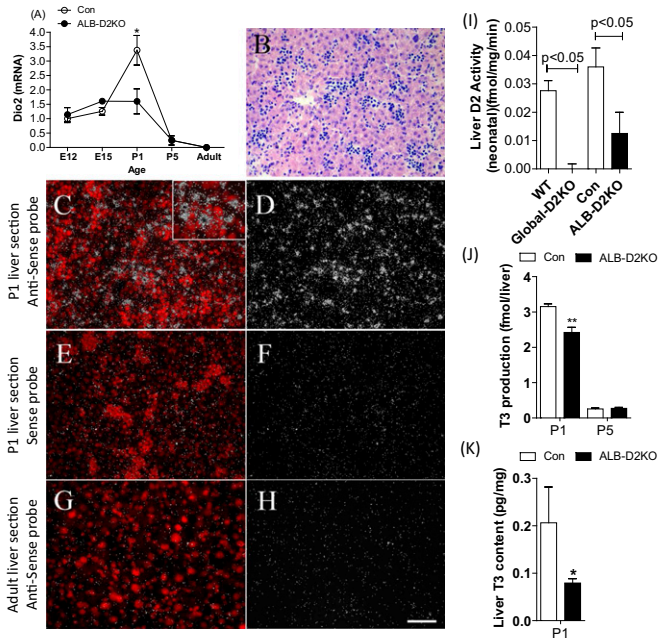

Fig. 1. Liver deiodinases in ALB-D2KO and control mice. (*A*) Relative Dio2 mRNA levels in embryonic (E12 and E15), neonatal (P1–P5) and adult livers. D2 mRNA levels are relative to 18S mRNA levels and normalized to E12. (*B*) Bright-field image of cresil violet- and eosin-counterstained P1 liver section. (*C–H*) Cresil violet-counterstained (*C*, *E*, and *G*) and dark-field (*D*, *F*, and *H*) images of D2 mRNA hybridization in mouse liver. (*C* and *D*) P1 mouse liver with D2-expressing cells distributed uniformly (higher-magnification view in *C*, *Inset*). (*E* and *F*) Background signal with sense probe in a P1 animal. (*G* and *H*) Adult hypothyroid mouse liver showing no signal after 6-wk exposure. (Scale bar: 50 μm.) (*I*) D2 activity in liver sonicates from neonatal ALB-D2KO and Global-D2KO mice (n = 5–7). (*J*) T3 production in intact hepatocytes of P1 and P5 animals (32). (*K*) Liver T3 content of P1 animals (32). All of the modifications are in supplanted material. Values are the mean ± SEM of three to seven independent samples. *P < 0.05, **P < 0.01 vs. controls.

Perinatal Liver D2 Affects the Expression of Genes Involved in Lipid Homeostasis. Thyroid hormone is known to affect the hepatic expression of genes involved in lipid homeostasis (9). Thus, we used qRT-PCR to measure the expression of candidate genes known to be T3-regulated and/or to play important roles in lipid homeostasis at different developmental and postnatal time points. No differences in gene expression during embryogenesis were observed between ALB-D2KO and controls (Fig. 2 *A* and *B*). However, P1 ALB-D2KO mice exhibited a 50–70% reduction in the expression of genes involved in (*i*) fatty acid synthesis: sterol regulatory element binding factor (Srebf) 1c and the key enzymes ATP citrate lyase (Acly), acetyl-CoA carboxylase (Acc), fatty acid synthase (Fasn; confirmed by an ∼50% decrease in protein levels; *SI Appendix*, Fig. S1*C*), thyroid hormone-responsive (Spot14), and stearoyl CoA desaturase 1 (Scd-1); (*ii*) triglyceride synthesis: mitochondrial glycerol-3-phosphate acyltransferase (Gpam), but not 1-acylglycerol-3-phosphate O-acyltransferase (Agpat) 2 or diacylglycerol oacyltransferase (Dgat) 2 (Fig. 2 *A* and *B*).

In contrast, liver peroxisome proliferator-activated receptor (PPAR) γ expression was higher in P1 ALB-D2KO mice compared with controls (Fig. 2*A*), whereas PPARα and carnitine palmitoyltransferase-1 (Cpt1) were not affected at all times (Fig. 2*A*). The expression of genes related to cholesterol metabolism was also affected by liver D2 inactivation, with a 40–60% reduction in expression level of Srebf2, low-density lipoprotein receptor (Ldlr), proprotein convertase subtilisin/kexin type 9 (Pcsk9), and 3-hydroxy-3-methyl-glutaryl-CoA reductase (HmgCoAR; Fig. 2*B*). The expression of LXR and cholesterol 7-alpha-monooxygenase (Cyp7a1) expression were approximately 20–50% higher in P1, although only the former reached statistical significance (Fig. 2*B*).

Adult ALB-D2KO Mouse Liver Exhibits a Distinct Transcriptome. All differences in gene expression identified in P1 (Fig. 2 *A* and *B*) dissipated in the adult ALB-D2KO mouse liver, with the notable exception of PPARγ mRNA levels, which were approximately one-half (Fig. 2*A*). T3 responsiveness also was preserved in the adult liver (*SI Appendix*, Fig. S3*K*). This analysis was broadened to an unbiased whole-transcript microarray approach that identified 165 altered genes at P <0.01, with 29 genes by >1.25-fold (*SI Appendix*, Fig. S4*A* and Dataset S1). A physiological context for these 165 genes was explored using gene set enrichment analysis (GSEA), which identified 31 gene sets modified in the ALB-D2KO with a normalized enrichment score (NES) >1.5 and a nominal P value <1% (*SI Appendix*, Dataset S2). These gene sets include "lipoprotein binding" and "carbohydrate transport" sets, as well as sets related to inflammation, cell signaling, cell structure, and DNA/cell cycle.

Despite its distinct gene expression profile, the adult ALB-D2KO mouse develops and reproduces normally (*SI Appendix*, Table S1) and is systemically euthyroid (*SI Appendix*, Fig. S1*D*). These animals have normal body weight evolution and indistinguishable weight of epididymal and interscapular BAT fat pads, brain, pancreas, and skeletal muscle compared with control animals (*SI Appendix*, Fig. S1 *E* and *F* and Table S2). Body composition and bone mineral density are also preserved in the ALB-D2KO mice (Fig. 3*E* and *SI Appendix*, Table S2). Of note, adult ALB-D2KO mice consistently ate approximately 20% more during the night cycle (*SI Appendix*, Fig. S1*G*), but their feces was of similar appearance and weight similarly as that of controls (*SI Appendix*, Fig. S1 *H* and *I*). The increased appetite is consistent with lower serum levels of pancreatic peptide YY and pancreatic polypeptide (PP) (*SI Appendix*, Table S13). In addition, their respiratory exchange ratio (RQ) values exhibited circadian rhythmicity (0.75–0.95) and were slightly lower during the day and higher at the beginning of the dark cycle (*SI Appendix*, Fig. S1*J*). Oxygen consumption (VO_2) (*SI Appendix*, Fig. S1*K*) and energy

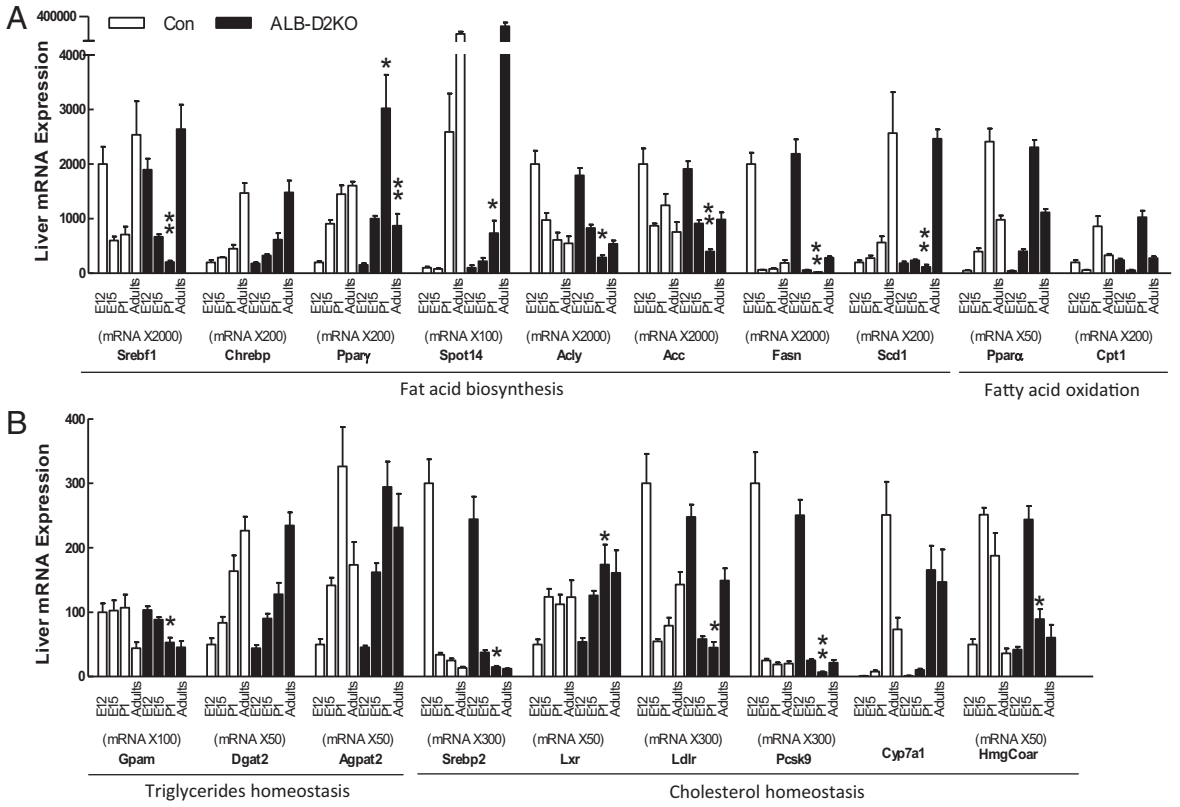

Fig. 2. Liver expression of lipid-related genes at different ages in ALB-D2KO and control mice. mRNA data are expressed as in Fig. 1*A*. Genes are grouped as fatty acid biosynthesis and fatty acid oxidation (*A*) and triglyceride homeostasis and cholesterol homeostasis (*B*). Values are mean ± SEM of four to eight independent samples. Gene abbreviations are as indicated in *SI Appendix*, Tables S11 and S12. $*P < 0.05$, $**P < 0.01$ vs. same-age control animals.

expenditure (EE) (*SI Appendix*, Fig. S1*L*) profiles exhibited the expected circadian rhythmicity, but no differences were observed between groups. Ambulatory movements (*x* and *y*) remained unaffected in the ALB-D2KO mice compared with controls (*SI Appendix*, Fig. S2 *A* and *B*).

Serum levels of glucose, insulin, C peptide2, leptin, and resistin, as well as tolerance to glucose, were all preserved in the ALB-D2KO animals (*SI Appendix*, Table S13 and Fig. S2*C*), as were serum cholesterol and triglyceride levels (Fig. 3 *H* and *I*). The liver weighed the same as that of controls (Fig. 3*D* and *SI Appendix*, Table S2), appeared normal (*SI Appendix*, Fig. S2*D*), and had a preserved microscopic structure (Fig. 3*J* and *SI Appendix*, Fig. S2*E*). Triglyceride (Fig. 3*F*) and cholesterol (Fig. 3*G*) levels in the ALB-D2KO livers were similar to those in controls.

DNA Methylation Profiling of Adult ALB-D2KO Liver. Given that liver D2 expression is perinatal but the adult ALB-D2KO liver exhibits a distinct gene expression profile, we hypothesized that the presence/absence of perinatal D2-generated T3 in hepatocytes permanently modifies gene expression and defines a phenotype that is carried forward through adulthood. Thus, we next performed genome-wide DNA methylation profiling by analyzing genomic DNA from the adult control and ALB-D2KO livers. Global DNA methylation exhibited a typical bimodal distribution pattern, without obvious global differences between control and ALB-D2KO samples (*SI Appendix*, Fig. S2 *F* and *G*); however, there were 3,552 differentially methylated local regions (DMRs) in 3,077 genes between the control and ALB-D2KO samples (*SI Appendix*, Dataset S3). These DMRs were subsequently analyzed using the Genomic Regions Enrichment of Annotations Tool (GREAT) platform, which assigns biological meaning to a set of noncoding genomic regions by analyzing the annotations of the nearby genes (Fig. 4). This led to the identification of 20 gene sets in the ALB-D2KO liver (*SI Appendix*, Table S3), including "lipid metabolic processes" and "hepatic fibrosis" sets in the top 10 (*SI Appendix*, Tables S4 and S5). The DMR-containing genes were also studied using the Molecular Signature Database (MSigDB), which identified 12 pathways (*SI Appendix*, Table S6), including "HDL-mediated lipid transport" (*SI Appendix*, Table S7).

These DMRs likely have physiological significance, considering that approximately 20% (713) map to genomic positions of active/repressed chromatin states as assessed using mouse ENCODE liver data coupled to ChromHMM. Here 437 DMRs were found to overlap with the markers of active chromatin state K4me1/3 + K36me3 (*SI Appendix*, Dataset S4) and were enriched in the "decreased circulating HDL cholesterol level" gene set, as well as 20 other developmental or inflammatory gene sets (*SI Appendix*, Tables S8 and S9). At the same time, 276 DMRs overlapped with K27me3, a marker of repressed chromatin state (Fig. 4 and *SI Appendix*, Dataset S5), and were enriched in eight developmental gene sets (*SI Appendix*, Table S10).

Adult ALB-D2KO Mice Are Resistant to Diet-Induced Obesity, Hypertriglyceridemia, and Liver Steatosis. Given that the adult ALB-D2KO mouse liver exhibits a transcriptome (*SI Appendix*, Datasets S1 and S2) and a methylome (*SI Appendix*, Dataset S3) that contain lipid-related gene sets, we next tested whether a more prominent metabolic phenotype would develop if these animals were switched to a high-fat diet (HFD-ALB-D2KO). Indeed, HFD-ALB-D2KO mice exhibited a remarkable ability to cope with lipid excess. Whereas HFD controls gained approximately 60% more body weight (Fig. 3*A*), fourfold more epididymal fat weight (Fig. 3*C*), and doubled liver weight (Fig. 3*D*) and amount of body fat (Fig. 3*E*), HFD-ALB-D2KO animals did not (Fig. 3 *A*, *C*, and *E*), even with a similar caloric intake (Fig. 3*B* and *SI Appendix*, Fig. S2*H*). In the HFD-ALB-D2KO animals, body fat increased by only ~30% (Fig. 3*E*). At the end of the HFD period, the RQ values in both the HFD-ALB-D2KO and HFD control

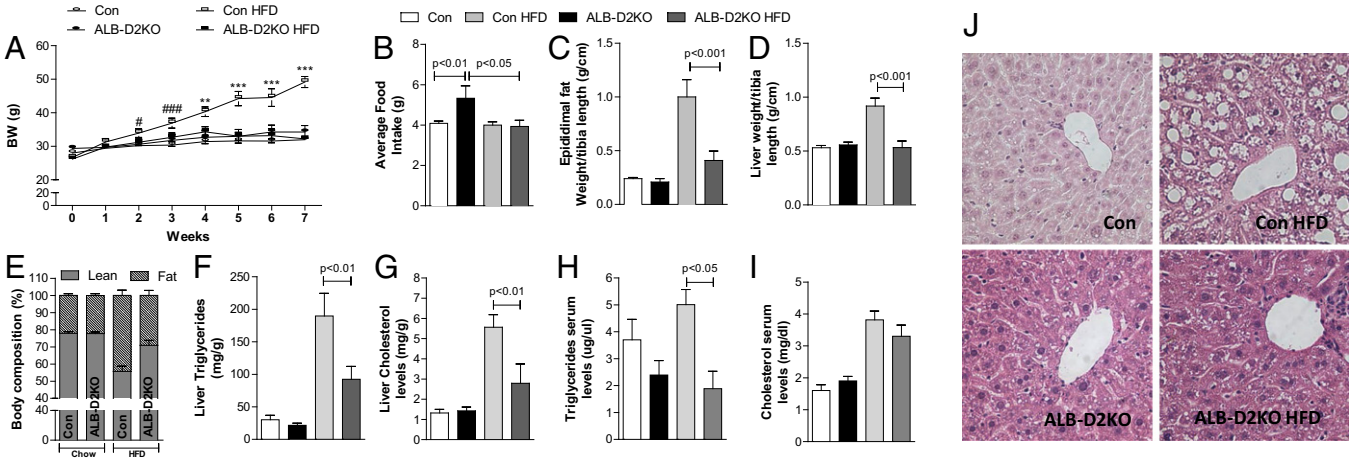

Fig. 3. Metabolic parameters in ALB-D2KO mice maintained on an HFD. (*A*) Body weight evolution. (*B*) Weekly food intake. (*C*) Epididimal fat pad weight. (*D*) Liver weight. (*E*) Body composition as measured by DEXA at 48 h before admission to CLAMS. (*F*) Liver triglycerides. (*G*) Liver cholesterol. (*H*) Serum triglycerides. (*I*) Serum cholesterol. (*J*) Representative liver section stained with H&E. (Original magnification, 40×.) All entries are mean ± SEM of four to six animals. $^{\#}P < 0.05$, $^{\#\#\#}P < 0.001$ vs. control; $^{***}P < 0.001$ vs. all groups.

mice had lost circadian rhythmicity while fluctuating between 0.75 and 0.85 (*SI Appendix*, Fig. S2*I*). Notably, nocturnal VO_2 (*SI Appendix*, Fig. S2*J*) and EE (*SI Appendix*, Fig. S3*A*) values were slightly elevated in the HFD-ALB-D2KO mice, indicating periods of accelerated metabolic rate. The HFD-ALB-D2KO mice exhibited no differences in BAT Ucp-1 and D2 mRNA levels (*SI Appendix*, Fig. S3 *B–D*) or in ambulatory activity (*SI Appendix*, Fig. S3 *E* and *F*).

Serum leptin levels were lower and serum resistin levels were higher in the HFD-ALB-D2KO animals (*SI Appendix*, Table S13). Whereas serum cholesterol was approximately doubled in both HFD groups (Fig. 3*I*), serum triglyceride levels were 2.5-fold lower in the HFD-ALB-D2KO mice compared with the HFD controls (Fig. 3*H*). Liver weight was approximately doubled in the HFD controls, but remain unchanged in the HFD-ALB-D2KO animals (Fig. 3*D*). In the HFD controls, liver steatosis was evident both anatomically (*SI Appendix*, Fig. S2*D*) and microscopically (Fig. 3*J* and *SI Appendix*, Fig. S2*E*), but no evidence of steatosis was observed in the HFD-ALB-D2KO livers (Fig. 3 *J* and *K* and *SI Appendix*, Fig. S2*D*). Of note, the liver content of cholesterol and triglycerides increased by approximately fivefold to sixfold in the HFD controls (Fig. 3 *F* and *G*), but remained unchanged in the HFD-ALB-D2KO mice (Fig. 3 *F* and *G*).

Major Differences Exist in the Liver Transcriptome of HFD-ALB-D2KO Mice and HFD Controls, Some of Which Are Associated with DNA Methylation. To define the molecular basis underlying the HFD-ALB-D2KO phenotype, we next sought to identify genes differentially expressed in the HFD-ALB-D2KO mice. To do so, we assessed liver expression of candidate genes involved in fatty acid, triglyceride, and cholesterol metabolism. Compared with the HFD control livers, Pparγ, Acc, Fasn, Scd1, and Gpam* (*denotes a DMR) mRNA levels were all lower in HFD-ALB-D2KO livers, whereas apoprotein A (Apoa) 1* mRNA levels were elevated (Fig. 5). This list was expanded with a microarray analysis of the HFD livers, which led us to identify 153 differentially expressed genes at $P < 0.01$, with 48 genes by >1.25-fold (*SI Appendix*, Fig. S4*B* and Dataset S6). These include three additional down-regulated lipid-related genes in the HFD-ALB-D2KO liver—sphingomyelin phosphodiesterase 3, neutral (Smpd3); 3-oxoacyl-ACP synthase, mitochondrial (Oxsm); and stearoyl-CoA desaturase 2 (Sdc2*)—as well as eight up-regulated lipid-related genes—apolipoprotein M (Apom), insulin-like growth factor binding protein 2 (Igfbp2), apolipoprotein L 9b (Apol9b), elongation of very long chain fatty acids protein 7 (Elovl7*), insulin-like growth factor 1(Igf1), ATP-binding cassette subfamily G member 1 (Abcg1*), ceramide synthase 5 (Cers5), and peroxiredoxin1 (Prdx1) (*SI Appendix*, Dataset S6). In fact, a subsequent GSEA of the 153 genes identified two lipid-related gene sets, "lipid homeostasis" and "lipid transport," as well as 17 other gene sets involved in cell signaling and the DNA/cell cycle, with an NES >1.5 and a nominal *P* value <1% (*SI Appendix*, Fig. S3*G* and Dataset S7).

The ALB-D2KO Liver Transcriptome in Response to HFD Is Limited and Is Partially Affected by DNA Methylation. To test whether the HFD-ALB-D2KO liver phenotype could be explained by a different transcriptional response to HFD (*SI Appendix*, Fig. S4 *C* and *D*, Dataset S8 vs. Dataset S9), we examined the liver expression of candidate genes and found that the HFD-induced expression of Srebf-1c*, Pparγ, Spot14*, Acly, Acc, Fasn, Gpam*, Agpat2, solute carrier family 27 (fatty acid transporter) member 5 (Slc27a5*), and phosphate cytidylyl-transferase 2, ethanolamine (Pcyt2) genes was weaker in the HFD-ALB-D2KO liver (Fig. 5). In contrast, HFD-induced expression of ATP-binding cassette transporter (Abca1*) and phospholipase A1 member A (Pla1a*) was stronger in the HFD-ALB-D2KO animals (Fig. 5).

Our microarray analyses indicated that in fact, 419 genes (199 genes >1.25-fold) were affected by the HFD in the control livers at $P < 0.01$ (*SI Appendix*, Dataset S8), compared with 212 genes (75 genes >1.25-fold) in the ALB-D2KO livers (*SI Appendix*, Dataset S9). Of note, not only the number, but also the identity, of these genes was markedly different, with only 10 overlapping genes in the control and ALB-D2KO responses to HFD (*SI Appendix*, Fig. S5 and Datasets S8 and S9).

To test the role played by DMRs in this different transcriptional response to the HFD, we crossed the 419 genes differentially

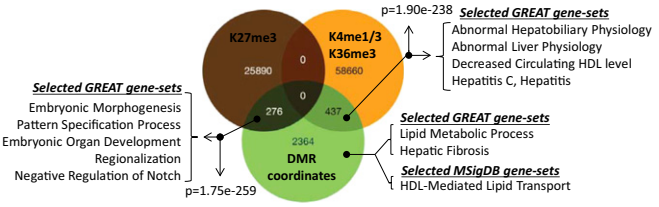

Fig. 4. Transcriptome and genome-wide DNA methylation profiling in adult ALB-D2KO mice. Venn diagram indicating overlapping between k4me1/3 + K36me3 (orange circle) or k27me3 (brown circle) containing histones and DMRs (green circle). Some of the gene sets contained in the overlapping areas (as identified by GREAT or MSigDB) are indicated. *P* values were calculated by a hypergeometric test in the R environment.

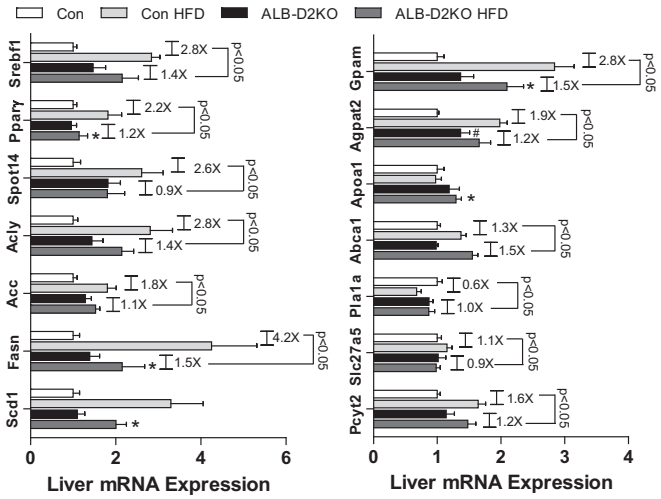

Fig. 5. Gene expression analysis in liver of ALB-D2KO animals maintained on an HFD. Liver mRNA levels of candidate genes are shown. The results are relative to 18S mRNA levels and normalized to control chow diet animals. Values are mean ± SEM of five to eight independent samples. Gene abbreviations are provided in *SI Appendix*, Tables S11 and S12. $^{\#}P < 0.05$ vs. respective chow diet control; $^{*}P < 0.05$ vs. respective HFD control.

expressed in the HFD controls (*SI Appendix*, Dataset S8) and the 212 genes differentially expressed in the HFD-ALB-D2KO mice (*SI Appendix*, Dataset S9) with the 3,552 DMRs (*SI Appendix*, Dataset S3), which identified 82 and 32 genes, respectively (*SI Appendix*, Fig. S5). Remarkably, Gpam* and lysocardiolipin acyltransferase-1 (Lclat1*) were among the genes up-regulated by the HFD in the controls animals, whereas Abcg1* was up-regulated by the HFD in the ALB-D2KO animals.

Discussion

Transcriptional regulation by thyroid hormone receptors is thought to be a reversible process controlled by T3 binding to the receptor (1). This involves covalent modifications of histones and chromatin structure, recruitment of RNA pol II complex and accelerated transcription. It also may involve control of the methylation status of the promoter, such as with Spot14 in the adult liver (24). Here we show that disruption of the brief neonatal surge in D2-mediated T3 signaling can (*i*) delay the expression of genes in neonatal liver involved in fatty acid, triglyceride, and cholesterol synthesis, and increase the expression of genes involved in bile acid synthesis; (*ii*) permanently modify the expression of approximately 165 genes in the adult liver; and (*iii*) reduce the number and types of genes induced by long-term HFD in the adult liver. Approximately 10–20% of the genes affected by perinatal D2 contain DMRs, indicating the involvement of T3-initiated epigenetic chromatin control.

Although many of the genes affected in P1 are normalized by adulthood, the adult ALB-D2KO liver retains a distinct transcriptome and methylome that involves broad aspects of hepatocyte function, including lipid metabolism (Fig. 4). These changes do not result in any significant metabolic phenotype, but they underlie major metabolic differences in response to prolonged HFD. Essentially, whereas the control liver exhibits a broad transcriptional response—approximately 400 genes—to HFD, favoring the synthesis of fatty acids and triglycerides (Srebf-1c*, Pparγ, Spot14*, Acly, Acc, Fasn, Scd1, Gpam*, Agpat2, Oxsm, Sdc2*, Slc27a5*, and Lclat1*), the HFD-ALB-D2KO liver response is limited—approximately 200 genes—associated with reverse cholesterol transport and lipase activity (Apoa1*, Apom, Apol9b, Abcg1*, Abca1*, and Pla1a*).

The present study suggests that during a brief time window, "modifiable lipid-related genes" in the liver are directly/indirectly susceptible to T3 signaling, which permanently affects their future ability to respond to physiological stimuli. This idea is supported by previous observations in mice that the first week after birth constitutes a "sensitive" period during which transient activation of thyroid hormone signaling can have permanent life-long effects, such as decreased hepatic EGF receptor number and body growth (25), increased adiposity (26), and precocious puberty (27). These effects can be seen after a short course of thyroid hormone administration, as well as in animals with targeted disruption of the type 3 deiodinase, which inactivates both T4 and T3 (27).

The D2-mediated epigenetic modifications in the liver are most notable in, but not limited to, gene sets involved in lipid metabolism. First, a number of differentially expressed genes and gene sets in the ALB-D2KO liver are/contain lipid-related genes (Fig. 2 *A* and *B* and *SI Appendix*, Datasets S1 and S2). Second, the DMRs are associated with lipid-related genes and gene sets (Fig. 4). Third, a number of differentially expressed genes in the HFD-ALB-D2KO livers are lipid-related, including those that overlap with the DMRs (Fig. 5 and *SI Appendix*, Figs. S3*G* and S4*B*). Fourth, the HFD-induced changes in ALB-D2KO liver transcriptome are much broader and include a large number of lipid-related gene sets (*SI Appendix*, Figs. S4 *C* and *D* and S5). Fifth, the dramatic metabolic phenotype exhibited by the ALB-D2KO animals in response to the HFD illustrates the physiological consequences of such mechanisms (Fig. 3).

The changes in the transcriptome were not exclusive to lipid-related genes, however. The fact that many other T3-modifiable gene sets were also identified in both the expression studies (*SI Appendix*, Datasets S1 and S2) and the methylome studies (*SI Appendix*, Dataset S3) indicates that D2-mediated control of gene transcription in the neonatal liver is a broader phenomenon, with clear implications for other aspects of liver physiology and/or pathophysiology.

The present findings also indicate that events occurring in the liver can control the susceptibility to diet-induced obesity. Previous studies have linked the development of diet-induced obesity to increased expression of lipogenic genes in the liver. Resistance to obesity in lean mice was associated with a reduction in liver expression of Scd-1 (28), a gene that was also decreased in the ALB-D2KO animals, along with many other lipogenic genes (Fig. 5). Taken together, these data support the hypothesis that a greater flux of fatty acids from the liver to peripheral tissues constitutes an important obesity mechanism; establishment of obesity is severely impaired if the lipogenic capacity of the liver is disrupted.

An apparent paradox is the observation of liver steatosis in the global-D2KO mice (21); however, this is attributed to increased sympathetic activity and lipolysis, which compensate for the global inactivation of D2 and the resulting defective BAT thermogenesis in these animals. Only the selective liver D2 inactivation unmasked the novel phenotype reported here. A transient elevation in D2-mediated T3 production in the perinatal mammalian liver permanently affects its transcriptome and defines the expression level and responsiveness of lipid-related genes throughout life through changes in the pattern of DNA methylation, which also defines the metabolic susceptibility to HFD. That this occurs via D2-mediated T3 production illustrates how deiodinase-mediated signals play major developmental and metabolic roles. It is likely that similar mechanisms occur in other D2-expressing developing tissues as well, including brain, BAT, and bone. Given that D2 is not expressed in the adult liver, the perinatal surge in D2 at the moment at which these genes are susceptible to permanent modifications makes the present mechanism unique.

Experimental Procedures

Animals. All experiments were approved by the local Institutional Animal Care and Use Committee at Rush University Medical Center and University of Miami School of Medicine. Mice with hepatocyte-specific Dio2 inactivation (ALB-D2KO) were obtained by crossing floxed D2 mice (*dio2*^{Flx}) (29) with mice expressing Cre-recombinase under the albumin promoter (Cre-ALB) [B6.Cg-Tg (Alb-cre)21Mgn/J; The Jackson Laboratory] (23). Cre-ALB served as a control in all experiments. GLOB-D2KO mice were obtained and maintained as described previously (30). All mice were male in a B6 background.

The mice were kept at room temperature (22 °C) under a 12-h dark/light cycle, and maintained on a chow diet (3.1 kcal/g; 2918 Teklad Global Protein rodent diet; Harlan) or HFD (4.5 kcal/g; TD 95121; Harlan) as indicated. The HFD experiments were performed in 8-wk old ALB-D2KO mice and littermate controls and lasted 7 wk. Animals were euthanized by asphyxiation in a CO_2 chamber.

Indirect Calorimetry. Animals were admitted to a comprehensive laboratory animal monitoring system (CLAMS; Columbus Instruments), kept at 22 °C, and studied as described previously (21). VO_2, RQ, EE, *x* and *y* ambulatory movement, and food consumption were monitored continuously. Lean body mass was measured at 48 h before the CLAMS studies by dual-energy X-ray absorptiometry (Lunar Pixi) (21).

Histology and in Situ Hybridization. Immediately after the mice were killed, liver fragments were processed for H&E staining. For the in situ testing, livers from P1 euthyroid and adult hypothyroid mice were quickly frozen in dry ice and then stored at −80 °C. The samples were processed as described previously (31), with modifications as detailed in *SI Appendix*.

Gene Expression Analysis. RNA was extracted using the RNeasy Kit (Qiagen) and quantified with a NanoDrop spectrophotometer. cDNA synthesis was performed with the First-Strand cDNA Synthesis Kit for RT-PCR (Roche) using 100 ng of total RNA. Genes of interest were measured by RT-PCR (StepOnePlus real-time PCR system; Applied Bioscience) using SYBR Green Supermix (Quanta Biosciences). Standard curves consisting of four or five points of serially diluted mixed experimental and control group cDNA were included. The coefficient of correlation was consistently >0.98, with an amplification efficiency of 80–110%. The primers used are listed in *SI Appendix*, Tables S11 and S12; 18S served as an internal control (*SI Appendix*, Fig. S3 *H–J*). Amplicon specificity was assessed by the melting curve.

Microarray Analysis. RNA was extracted with the RNeasy Lipid Tissue Mini Kit (Qiagen). Liver RNA obtained from ALB-D2KO and control mice were processed for microarray at the Joslin Diabetes Center Genomics Core Laboratory. Gene expression was evaluated using Affymetrix Mouse Gene 2.0 ST arrays. Gene expression data were preprocessed using Affymetrix Expression Console software. Differential expression analysis was performed with Affymetrix Transcriptome Analysis Console software to identify individual genes, and Gene Ontology analysis was used to determine differences in enrichment of gene sets between phenotypes (GSEA, Broad Institute). Details are provided in *SI Appendix*.

Methylome Analysis. Two enrichment-based methods, methylation-dependent immunoprecipitation followed by sequencing (MeDIP-seq) and methylation-sensitive restriction enzyme digestion followed by sequencing (MRE-seq), were integrated. Two computational algorithms, M&M and methylCRF, were used to obtain a genome-wide CpG methylation profile. MeDIP and MRE sequencing libraries were constructed as described previously. Detailed descriptions of the preparation of MeDIP and MRE sequencing libraries and analysis are provided in *SI Appendix*.

Biochemical Analyses. Serum was processed using a MILLIPLEX rat thyroid hormone panel kit and MILLIPLEX mouse metabolic hormone magnetic bead panel kit (Millipore) read on a Bio-Plex multiplex system (Bio-Rad). Liver triglyceride and cholesterol levels were measured in ∼200-mg liver fragments after homogenization and extraction in chloroform/methanol (2:1) and 0.05% sulfuric acid (21). Deiodinase assays were as described previously, using 100 nM T4 for background activity (32).

Statistical Analysis. All data are expressed as mean ± SEM and were analyzed using GraphPad Prism. One-way ANOVA was used to compare more than two groups, followed by the Student–Newman–Keuls test to detect differences among groups. The Student *t* test was used when only two groups were part of the experiment; $P < 0.05$ was used to reject the null hypothesis.

ACKNOWLEDGMENTS. We thank Dr. Maria de Jesus Obregon for providing the T3 antibody and invaluable expertise in measuring T3 content in liver. This work was supported by National Institute of Diabetes and Digestive and Kidney Diseases Grants R01 65055 and R01 37021; NIH Grants 5R01HG007354, 5R01HG007175, 5R01ES024992, and 2U01CA200060; American Cancer Society Research Scholar Grant RSG-14-049-01-DMC; the Hungarian Brain Research Program; and a Lendület Grant from the Hungarian Academy of Sciences and Coordenadoria de Apoio a Pesquisa, Brazil.

1. Brent GA (2012) Mechanisms of thyroid hormone action. *J Clin Invest* 122(9):3035–3043.
2. Andersen S, Bruun NH, Pedersen KM, Laurberg P (2003) Biologic variation is important for interpretation of thyroid function tests. *Thyroid* 13(11):1069–1078.
3. Huang SA, Bianco AC (2008) Reawakened interest in type III iodothyronine deiodinase in critical illness and injury. *Nat Clin Pract Endocrinol Metab* 4(3):148–155.
4. Gereben B, Zeöld A, Dentice M, Salvatore D, Bianco AC (2008) Activation and inactivation of thyroid hormone by deiodinases: Local action with general consequences. *Cell Mol Life Sci* 65(4):570–590.
5. Bianco AC, Silva JE (1987) Intracellular conversion of thyroxine to triiodothyronine is required for the optimal thermogenic function of brown adipose tissue. *J Clin Invest* 79(1):295–300.
6. Simonides WS, et al. (2008) Hypoxia-inducible factor induces local thyroid hormone inactivation during hypoxic-ischemic disease in rats. *J Clin Invest* 118(3):975–983.
7. Olivares EL, et al. (2007) Thyroid function disturbance and type 3 iodothyronine deiodinase induction after myocardial infarction in rats: A time course study. *Endocrinology* 148(10):4786–4792.
8. Jo S, et al. (2012) Neuronal hypoxia induces Hsp40-mediated nuclear import of type 3 deiodinase as an adaptive mechanism to reduce cellular metabolism. *J Neurosci* 32(25):8491–8500.
9. Oppenheimer JH, et al. (1987) Advances in our understanding of thyroid hormone action at the cellular level. *Endocr Rev* 8(3):288–308.
10. Cavallo-Perin P, et al. (1988) Insulin resistance in Graves' disease: A quantitative in-vivo evaluation. *Eur J Clin Invest* 18(6):607–613.
11. Dimitriadis GD, Raptis SA (2001) Thyroid hormone excess and glucose intolerance. *Exp Clin Endocrinol Diabetes* 109(Suppl 2):S225–S239.
12. Flores-Morales A, et al. (2002) Patterns of liver gene expression governed by TRbeta. *Mol Endocrinol* 16(6):1257–1268.
13. Feng X, Jiang Y, Meltzer P, Yen PM (2000) Thyroid hormone regulation of hepatic genes in vivo detected by complementary DNA microarray. *Mol Endocrinol* 14(7):947–955.
14. Findlay KA, Kaptein E, Visser TJ, Burchell B (2000) Characterization of the uridine diphosphate-glucuronosyltransferase–catalyzing thyroid hormone glucuronidation in man. *J Clin Endocrinol Metab* 85(8):2879–2883.
15. Schneider MJ, et al. (2006) Targeted disruption of the type 1 selenodeiodinase gene (Dio1) results in marked changes in thyroid hormone economy in mice. *Endocrinology* 147(1):580–589.
16. Gereben B, et al. (1999) Cloning and expression of the chicken type 2 iodothyronine 5′-deiodinase. *J Biol Chem* 274(20):13768–13776.
17. Stilborn SS, Manzon LA, Schauenberg JD, Manzon RG (2013) Thyroid hormone deiodinase type 2 mRNA levels in sea lamprey (*Petromyzon marinus*) are regulated during metamorphosis and in response to a thyroid challenge. *Gen Comp Endocrinol* 183:63–68.
18. Kwakkel J, et al. (2014) A novel role for the thyroid hormone-activating enzyme type 2 deiodinase in the inflammatory response of macrophages. *Endocrinology* 155(7):2725–2734.
19. Kalaany NY, et al. (2005) LXRs regulate the balance between fat storage and oxidation. *Cell Metab* 1(4):231–244.
20. Christoffolete MA, et al. (2010) Regulation of thyroid hormone activation via the liver X-receptor/retinoid X-receptor pathway. *J Endocrinol* 205(2):179–186.
21. Castillo M, et al. (2011) Disruption of thyroid hormone activation in type 2 deiodinase knockout mice causes obesity with glucose intolerance and liver steatosis only at thermoneutrality. *Diabetes* 60(4):1082–1089.
22. Fonseca TL, et al. (2014) Tissue-specific inactivation of type 2 deiodinase reveals multilevel control of fatty acid oxidation by thyroid hormone in the mouse. *Diabetes* 63(5):1594–1604.
23. Weisend CM, Kundert JA, Suvorova ES, Prigge JR, Schmidt EE (2009) Cre activity in fetal albCre mouse hepatocytes: Utility for developmental studies. *Genesis* 47(12):789–792.
24. Wong NC, Schwartz HL, Strait K, Oppenheimer JH (1989) Thyroid hormone-, carbohydrate, and age-dependent regulation of a methylation site in the hepatic S14 gene. *Mol Endocrinol* 3(4):645–650.
25. Alm J, Lakshmanan J, Hoath S, Fisher DA (1988) Neonatal hyperthyroidism alters hepatic epidermal growth factor receptor ontogeny in mice. *Pediatr Res* 23(6):557–560.
26. Moura EG, et al. (2008) Thyroid function and body weight programming by neonatal hyperthyroidism in rats: The role of leptin and deiodinase activities. *Horm Metab Res* 40(1):1–7.
27. Tsai CE, et al. (2002) Genomic imprinting contributes to thyroid hormone metabolism in the mouse embryo. *Curr Biol* 12(14):1221–1226.
28. de Fourmestraux V, et al. (2004) Transcript profiling suggests that differential metabolic adaptation of mice to a high-fat diet is associated with changes in liver to muscle lipid fluxes. *J Biol Chem* 279(49):50743–50753.
29. Fonseca TL, et al. (2013) Coordination of hypothalamic and pituitary T3 production regulates TSH expression. *J Clin Invest* 123(4):1492–1500.
30. Christoffolete MA, et al. (2004) Mice with targeted disruption of the Dio2 gene have cold-induced overexpression of the uncoupling protein 1 gene but fail to increase brown adipose tissue lipogenesis and adaptive thermogenesis. *Diabetes* 53(3):577–584.
31. Gereben B, Pachucki J, Kollár A, Liposits Z, Fekete C (2004) Ontogenic redistribution of type 2 deiodinase messenger ribonucleic acid in the brain of chicken. *Endocrinology* 145(8):3619–3625.
32. Bianco AC, et al. (2014) American Thyroid Association guide to investigating thyroid hormone economy and action in rodent and cell models. *Thyroid* 24(1):88–168.